Inorganic Chemistry Communications 176 (2025) 114238

Contents lists available at ScienceDirect

Inorganic Chemistry Communications

journal homepage: www.elsevier.com/locate/inoche

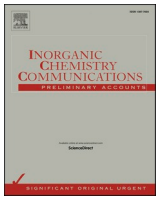

Short communication

Easy access to VO_2 nanostructures with controllable morphologies

Siyang Han [a], Yue Lu [a], Weichen Han [a], Jingang Zheng [a], Hongwei Zhao [a], Han Zhang [a], Guangshen Jiang [a], Lixiang Li [a], Weimin Zhou [a], Baigang An [a,*], Chengguo Sun [a,b,*]

[a] School of Chemical Engineering, University of Science and Technology, Liaoning, Anshan 114051, China
[b] School of Chemical Engineering, Nanjing University of Science and Technology, Nanjing 210094, China

ARTICLE INFO

Keywords:
VO_2 nanostructures
Surfactants
Reducing agents
Controllable morphologies
Electrochemical kinetics

ABSTRACT

Vanadium dioxide (VO_2) has been widely investigated as electrochemical materials due to its reversible, ultrafast and multi-stimulus response phases transition. The morphological diversity of VO_2 can trigger the fluctuant electrochemical property, thereby researchers devote to synthesize VO_2 with controlled nanostructures. However, development of green solvothermal method to prepare the various morphologies of VO_2 materials with water as solvent is still facing great challenges. Here we have synthesized a series of configurational VO_2 including nanowires, nano-hollow spheres, nano-ellipsoids, nano-flowers, nano-spheres and nano-solid spheres by controlling surfactants/reducing agents in the presence of water. Both spherical and ellipsoidal VO_2 are corresponding to D phase, other structures are consistent with B phase. Their specific surface areas range from 4 to 30 m^2/g. The electrochemical performance indicates that spherical VO_2 as an electrode has a higher surface Redox kinetic than that of VO_2 nanostructures.

Low-dimensional nanostructures including nanorods, nanowires, nanoflowers, nanospheres, etc, remain a major concern due to their special optical and electrical properties [1,2]. Vanadium oxides as well-known prototype materials have been widely studied for their interesting physical properties [3,4]. Among the numerous vanadium oxides, vanadium dioxide (VO_2), one of the semiconductors with tunneled structure, has good application prospects in the field of energy storage [5]. For example, it is used as cathode materials in aqueous zinc-ion batteries (ZIBs) [6,7], ammonium-ion batteries (AIBs) [8–10], and as anode electrode material in supercapacitors [11]. In low-cost ZIBs, benefiting from variable vanadium valence, VO_2 works as a cathode material that facilitates the insertion and extraction capabilities of Zn^{2+}, which contributes to high specific capacity (645 mAh/g) [6,7]. However, development of rechargeable batteries using VO_2 as cathode materials are still facing great challenges owing to different morphological structures of VO_2 contribute different capacities, for example, at a current density of 10 A/g, the metal-doped VO_2 nanoflowers present a high capacity of 336 mAh/g in aqueous ZIBs [12]. The tunnel-oriented VO_2 nanobelts, hollow VO_2 nanospheres, and the VO_2 nanoflakes with petal-shaped folds as cathodes vary considerably to 344.8 mAh/g, 262.0 mAh/g, and 201.3 mAh/g, respectively [13–15]. Therefore, the design and preparation of VO_2 materials with controllable morphologies have a profound significance for development of vanadium-based materials.

As well described in the literature, some remarkable achievements have made for preparing VO_2 with large specific surface area and different pore sizes by chemical vapor deposition (CVD) [16], pulsed laser deposition (PLD) [17], solvothermal methods [18], thermal decomposition [19], and hydrothermal synthesis [20], yet there are also limitations and contradictions in experimental methods. CVD methods suffer from a few drawbacks including high equipment costs, the utilization of toxic gases (such as silane and ammonia) [16]. PLD has a slow average deposition rate, unfavorable for large-area deposition [17]. The method of thermal decomposition is usually carried out at high temperatures ($\geq$800) [19]. In contrast, solvothermal methods have the advantages of low energy consumption and controllable particle shape [18]. Specifically, the products prepared by hydrothermal process has uniform physical phase, good crystallization and controllable shape [20]. However, development of green solvothermal method to prepare the various morphologies of VO_2 materials with water as solvent is still facing great challenges.

Herein, we prepared the various morphologies of VO_2 materials including nanowires (V-NW), nano-hollow spheres (V-NH), nano-ellipsoids (V-NE), nanoflowers (V-NF), nanospheres (V-NS), and nano-solid spheres (V-NSS) by hydrothermal synthesis. The whole operation process was handed with water as primary solvent. By adding different surfactants (such as sodium dodecyl sulfate, polyvinylpyrrolidone,

* Corresponding authors.
E-mail addresses: bgan@ustl.edu.cn (B. An), sunyangguo2004@163.com (C. Sun).

https://doi.org/10.1016/j.inoche.2025.114238
Received 18 November 2024; Received in revised form 2 January 2025; Accepted 1 March 2025
Available online 3 March 2025

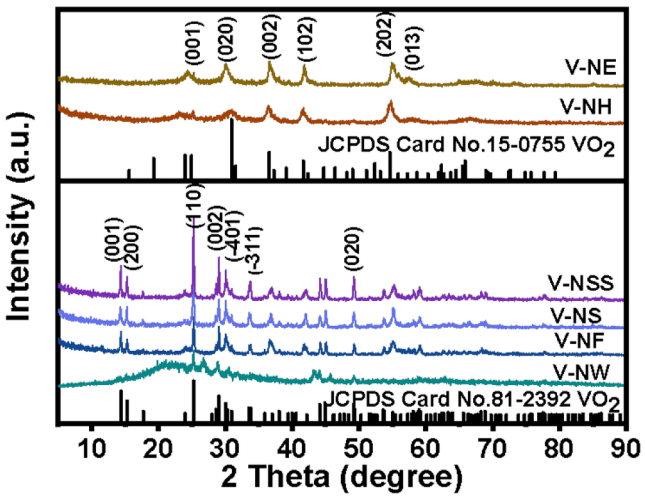

Fig. 1. Various XRD patterns of the VO_2 nanostructures.

NH_4HCO_3), the morphologies of VO_2 can be controlled from V-NF, V-NS, V-NE to V-NSS. Their electrochemical performance was investigated by Cyclic voltammetry (CV), which further analysed their structure contribution to the ability of capacitance and diffusion effects. The V-NS has higher surface Redox kinetics and rate capacity superior to that of other structured cathode materials.

The XRD patterns of the prepared VO_2 structure are shown in Fig. 1. The diffraction peaks of V-NW, V-NF, V-NS, and V-NSS are perfectly indexed to the orthorhombic phase VO_2 with high crystallinity (JCPDS card No. 81-2392). Their phases are well crystallized, and no other vanadium oxides were observed. Some preferential orientation in the (110) direction was observed for the monoclinic VO_2 samples [21]. On the amplified XRD pattern, it can be observed that the (110) peaks of V-NF, V-NS, V-NSS, and V-NW are offset, which corresponds to the shift of the (110) crystal plane spacing of different samples (Fig. S1). In contrast, the characteristic diffraction peaks of V-NE, V-NH are well indexed to the D phase of VO_2 (JCPDS NO. 15-0755) [22].

To visualize the morphology of VO_2 materials, Fig. 2 shows their scanning electron microscope (SEM) images and energy dispersive spectrometer (EDS) elemental mapping. It can be found that all prepared VO_2 materials are highly monodisperse. During the hydrothermal synthesis process of VO_2 nanostructures, we find that the morphologies can be affected by reductant with V_2O_5 as substrate and water as solvent. Fig. 2a shows a typical SEM image of VO_2 nanostructures synthesized with *n*-butanol as a reductant at 220 ℃. V-NW grew in an ordered manner with wide diameter ranging from 100 to 400 nm. The corresponding TEM image (Fig. S4a) shows the non-hollow structure. The high-resolution TEM (HRTEM) image of V-NW (Fig. S4c) indicates that the nanowire is single crystal, and the lattice spacing is 0.364 nm corresponding to *d* spacing of the (1 1 0) plane of monoclinic VO_2 (B) [21]. When the reductant *n*-butanol is replaced by methanol, V-NH structure was obtained. The SEM image shows that the prepared V-NH samples are in the form of nanospheres (Fig. 2d). According to the magnified SEM image, it can be observed that V-NH is are assembled from many rice-like nanorods (Fig. S3a–b). The corresponding TEM image of V-NH confirms the nanospheres are hollow structure with a spherical core of about 500 nm in diameter and a shell of about 50 nm in thickness (Fig. S3b). From the HRTEM image, the lattice spacing is 0.260 nm, which corresponds to the (002) face of VO_2 (D) (Fig. S4f) [22].

To obtain other structural VO_2, various surfactants including (SDS/PVP/NH_4HCO_3) were adopted to the reaction system to control VO_2

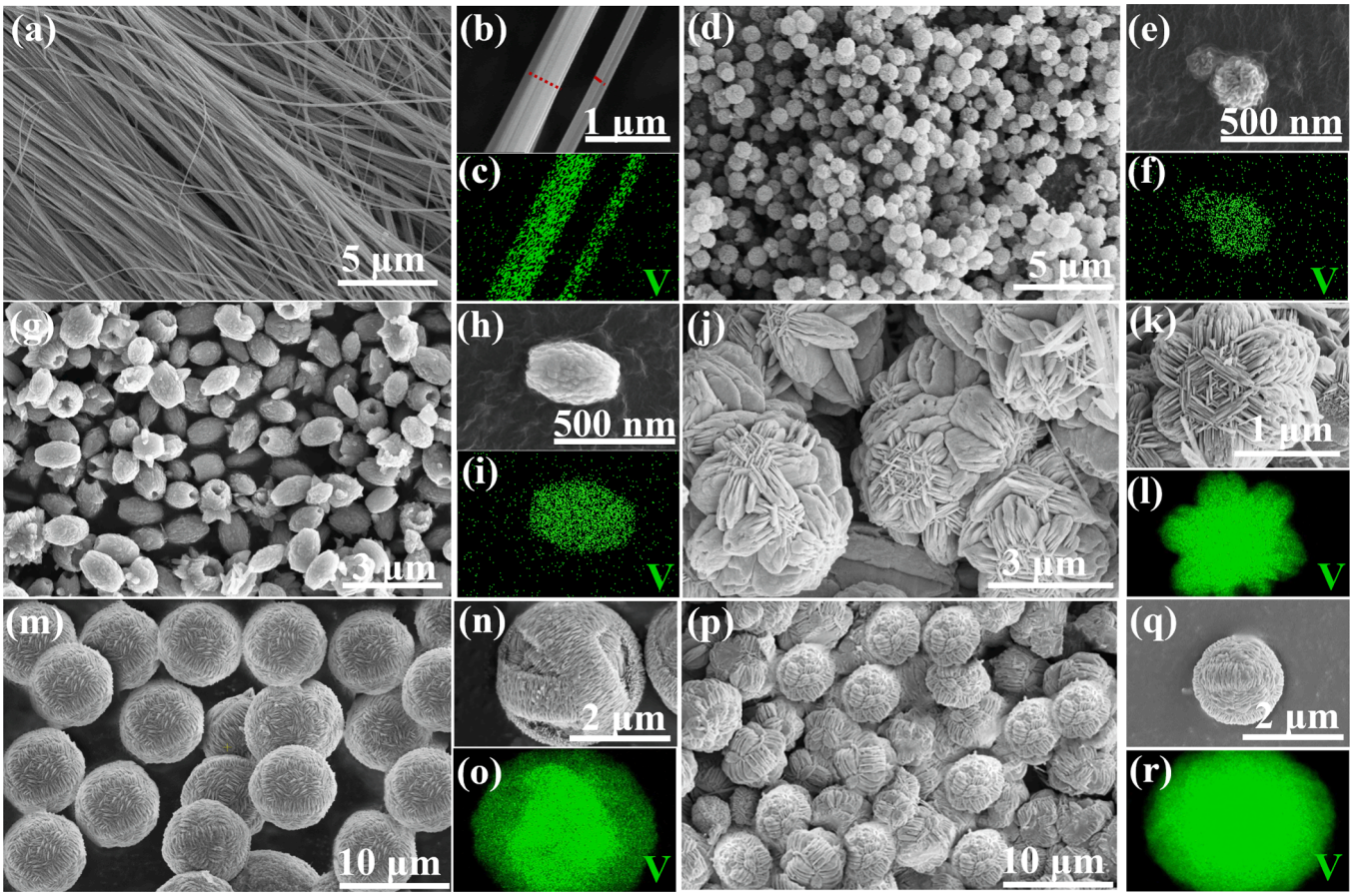

Fig. 2. Various SEM images and elemental mapping images of VO_2 nanostructures; (a–c) V-NW; (d–f) V-NH; (g–i) V-NE; (j–l) V-NF; (m–o) V-NS; (p–r) V-NSS.

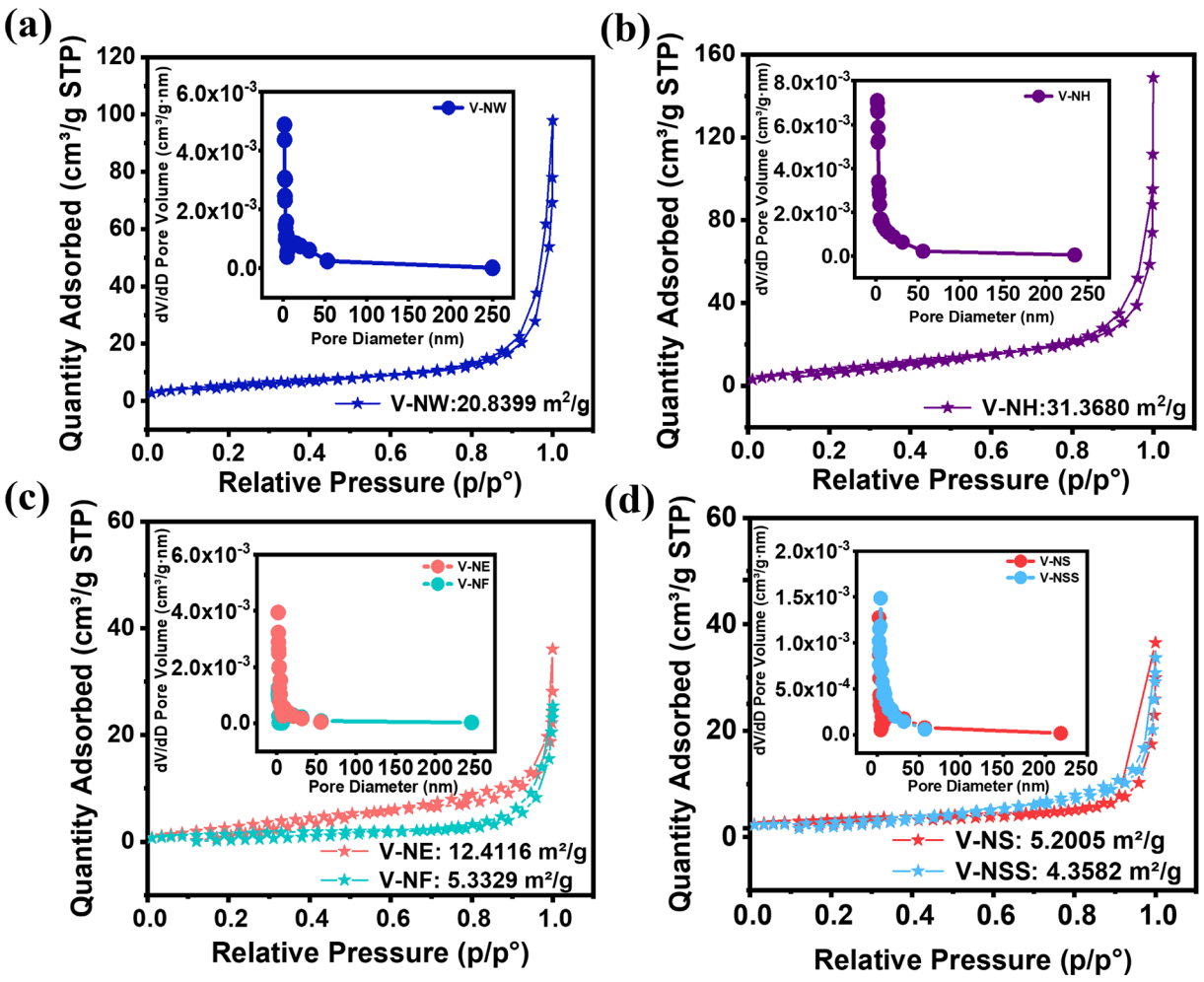

Fig. 3. (a) N_2 adsorption–desorption isotherm curves and pore size distribution curves of the (a) V-NW; (b) V-NH. (c) V-NE; V-NF; (d) V-NS; V-NSS.

morphologies. In the presence of PVP, V-NE samples were prepared. The morphology of V-NE is arranged in a uniform ellipsoid shape with a wide diameter of 1.4 μm (Fig. 2g). Interestingly, the SEM image shows that the ellipsoidal structure seems hollow from front to back. However, the TEM image of V-NE confirms the solid ellipsoid (Fig. S4g). From the HRTEM image, we can observe that its lattice spacing is 0.256 nm (Fig. S4i), which also corresponds to the (002) face of VO_2 (D) [22]. When the surfactant changed from PVP to SDS, V-NF was obtained. As shown in Fig. 2j, it reveals that the surface of V-NF has a petal-like structure with a diameter distribution between 2.4 and 2.6 μm. The V-NF is composed of many sheets from the enlarged view (Fig. 2k), and the TEM image of V-NF is solid structure (Fig. S4j). The HRTEM image of V-NF (Fig. S4l) indicates that the lattice spacing is 0.362 nm, corresponding to d spacing of the (1 1 0) plane of monoclinic VO_2 (B) [21]. Unexpectedly, we found that reaction time can also affect the morphology of the material. After the reaction time changed from 4 to 6 h, the V-NF is transformed into V-NS. The structure of V-NS is formed by the accumulation of many small nanosheets (Fig. 2m and Fig. S3c). Among all the nanostructured VO_2 prepared, V-NS has the largest diameter, ranging from 7.2 to 7.6 μm, and the TEM image shows that the V-NS structure is solid (Fig. S4m). The lattice spacing of V-NS is 0.351 nm corresponding to the (1 1 0) plane of VO_2 (B) (Fig. S4o) [21]. Furthermore, with the help of NH_4HCO_3, we obtained large diameter V-NSS. Although the obtained V-NSS is also a solid sphere structure, the morphology is different from that of V-NS. The SEM image of V-NSS demonstrates that V-NSS is a flower-like nanosphere composed of many nanosheets (Fig. 2p and Fig. S3d). Their diameters are mainly between 6.0 and 6.6 μm, and the TEM image confirms their solid structure (Fig. S4p). Moreover, the EDS elemental mapping of all materials demonstrates the uniform distribution of the V and O elements, which further verifies the successful fabrication of different morphologies of VO_2 (Fig. 2 and Fig. S2).

Thermogravimetric analysis (TGA) was conducted to investigate the phase transition of various VO_2 materials under air atmosphere. As shown in Fig. S5, from 30 to 350 °C, about 3 ~ 5 % weight loss was mainly attributed to volatilization of residual solvent, and decomposition of surfactants. When the temperature was elevated from 350 to 600 °C, the significant increase of sample weight was presented. The results indicated that the VO_2 is oxidized to V_2O_5 [23], the phase transition occurred along with the increase in temperature. To further verify the structure transformation, the V-NH materials were calcined at 600 ℃ in air atmosphere and characterized by XRD. As shown in Fig. S6 and its diffraction peaks is completely directed to the orthorhombic phase V_2O_5 with high crystallinity (JCPDS card No. 41-1426), which is consistent with the above analysis of TG curves [23].

The N_2 adsorption–desorption isotherms measurement was adopted to investigate the Brunauer-Emmett-Teller (BET) surface area and pore size distribution of the samples. According to the adsorption–desorption curves in Fig. 3, it can be seen that the specific surface area of the prepared samples ranges from 4 to 30 $m^2\ g^{-1}$, in detail, the specific surface area of V-NH can reach up to 31.3 $m^2\ g^{-1}$ (Fig. 3b). V-NF, V-NS and V-NSS have the low the specific surface area of 5.3, 5.2 and 4.3 $m^2\ g^{-1}$ (Fig. 3c–d), respectively. Both V-NW and V-NE have the moderate the specific surface area of 20. 8 and 12.4 $m^2\ g^{-1}$, respectively (Fig. 3a and

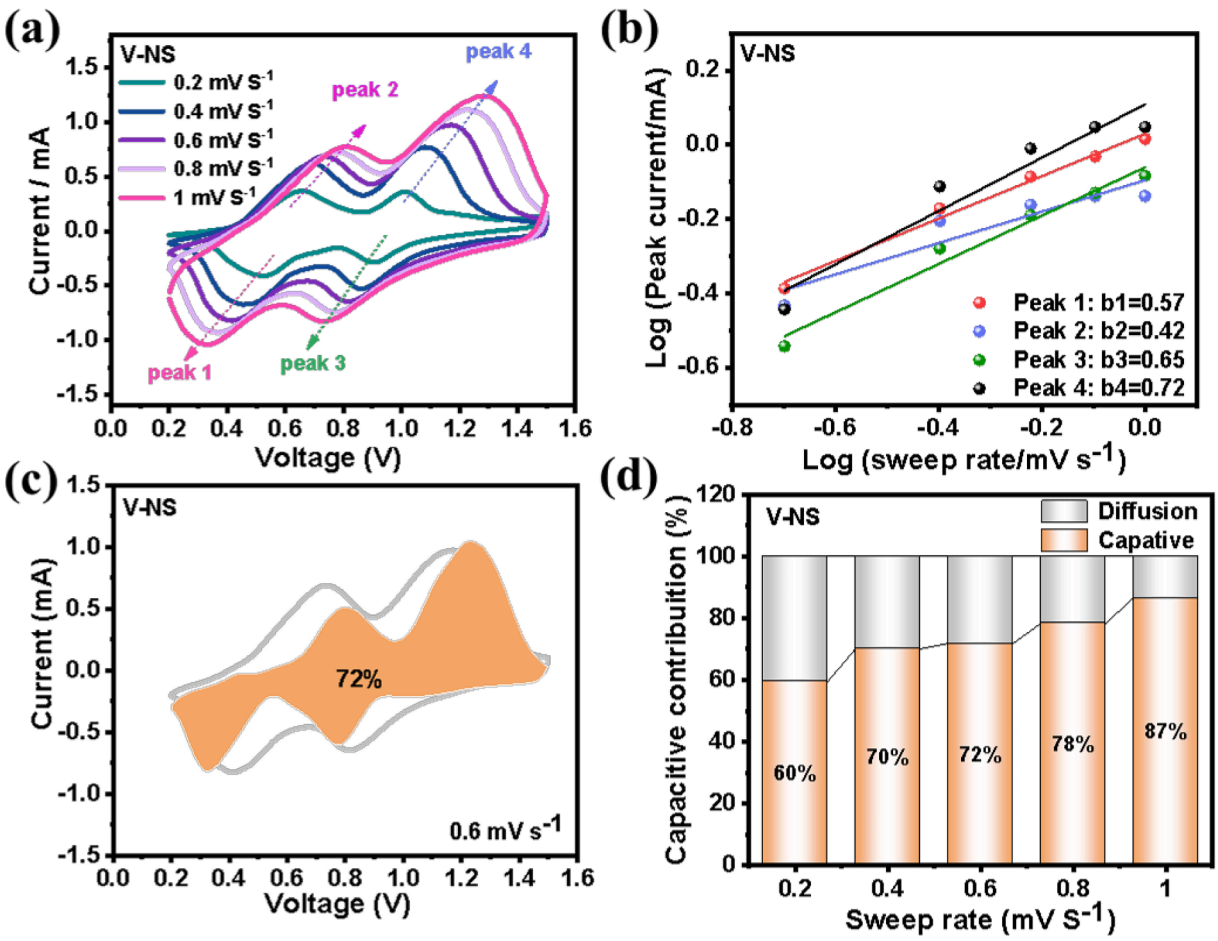

Fig. 4. (a) CV curves of V-NS electrode at various scan rates. (b) log (peak current) versus log (sweep rate) plots according to the CV data at selected oxidation/reduction peaks. (c) CV curve of the V-NS electrodes with capacity separation at 0.6 mV s^{-1}. (d) The capacitive contributions of V-NS electrode at different scan rates.

c). Fig. 3 also shows their pore size distribution, it is concluded that the prepared VO_2 with different morphologies are predominantly mesoporous [15].

To further analyze electrochemical activity of the prepared VO_2 nanostructures, the cyclic voltammetry (CV) tests were measured in electrolyte of 2 M $Zn(OTf)_2$ with a scan rate of 0.2 mV s^{-1}. Two pairs of redox peaks for all samples can be clearly observed in initial three cycles (Fig. S7), implying that the insertion/extraction of Zn^{2+} is a multistep process [24]. To evaluate the effect of morphology on diffusion coefficient of Zn^{2+} in VO_2 nanostructures, the electrochemical kinetics of Zn^{2+} in VO_2 nanostructures at a series of scanning rates from 0.2 to 1.0 mV s^{-1} were measured (Fig. 4a and Fig. S8) and the capacitive effect of the battery system is calculated. The detailed calculation method is given in the support information. The b values of VO_2 with different nanostructures are shown in Fig. 4b and Fig. S9. In general, when the b value is close to 0.5, it illustrates the Zn^{2+} insertion process dominates, whereas the b value approaches 1.0, it indicates a capacitive-controlled dominant process. We conclude that the electrochemical process of V-NW, V-NH, V-NE and V-NF electrode is dominated by the insertion of Zn^{2+}, while the electrochemical process of V-NS and V-NSS electrode is the mixed mode of ion insertion and capacitive-controlled process [25]. Among them, the b values of V-NS electrode are much higher than that of other nanostructured electrodes, indicating the faster ion diffusion kinetics in V-NS electrode. We also calculate the distribution of capacitance contribution to the total capacity of VO_2 with different nanostructures, and specific calculations are given in the Supporting Information. At scan rates of 0.2, 0.4, 0.6, 0.8 and 1.0 mV s^{-1}, the capacitive ratios for V-NS electrode are 60 %, 70 %, 72 %, 78 % and 87 %, respectively, which is much higher than that of other electrodes, suggesting the electrochemical process in V-NS electrode with faster ion transfer kinetics (Fig. 4c, d, Fig. S10 and S11) [26].

In summary, we have demonstrated a facile and flexible method-hydrothermal synthesis to synthesize various VO_2 nanostructures. By adjusting the components of the solution, V-NW and V-NH are obtained. By controlling the type of surfactant, we fabricate three different VO_2 morphologies including V-NF, V-NE and V-NS. Interestingly, VO_2 is transformed from V-NF to V-NSS by changing reaction time in the presence of SDS. Moreover, the method of preparing VO_2 can be scaled up for production. The electrochemical behavior of the prepared VO_2 shows that VO_2 with different morphologies prepared in this work are capable of storing Zn^{2+}.

Declaration of competing interest

The authors declare that they have no known competing financial interests or personal relationships that could have appeared to influence the work reported in this paper.

Acknowledgements

This work is supported by the National Natural Science Foundation of China (No. 52371224, 51972156, 22109061), the Fundamental Research Funds for the Liaoning Universities (No. 222410146062, 222410146075), and the Nature Science Foundation of Liaoning Province (No. 2022-BS-283).

Appendix A. Supplementary data

Experimental materials and methods, EDS elemental mapping of O, TEM and HRTEM images, TG curves, XRD pattern, CV curves and comparison of capacitance effect of different nanostructures. Supplementary data to this article can be found online at https://doi.org/10.1016/j.inoche.2025.114238.

Data availability

No data was used for the research described in the article.

References

[1] M. Zeng, H.H. Yin, K. Yu, Synthesis of V_2O_5 nanostructures with various morphologies and their electrochemical and field-emission properties, Chem. Eng. J. 188 (2012) 64–70.

[2] X.L. Li, X.J. Chen, X.Y. Chen, C.L. Han, C.W. Shi, Hydrothermal synthesis and characterization of VO_2 (B) nanorods array, J. Cryst. 309 (2007) 43–47.

[3] Y.J. Ke, X.L. Wen, D.Y. Zhao, R. Che, Q. Xiong, Y. Long, Controllable fabrication of two-dimensional patterned VO_2 nanoparticle, nanodome, and nanonet arrays with tunable temperature-dependent localized surface plasmon resonance, ACS Nano 11 (2017) 7542–7551.

[4] C.X. Cao, Y.F. Gao, L.T. Kang, H.J. Luo, Self-assembly and synthesis mechanism of vanadium dioxide hollow microspheres, CrstEngComm 12 (2010) 4048–4051.

[5] M.S. Liu, B. Su, Y. Tang, X.C. Liang, A.B. Yang, Recent advances in nanostructured vanadium oxides and composites for energy conversion, Adv. Energy Mater. 7 (2017) 1700885.

[6] L.S. Wu, M.H. Zhang, W. Xu, Y.F. Dong, Recent advances in carbon materials for flexible zinc ion batteries, New Carbon Mater. 37 (2022) 827–851.

[7] X.Y. Dou, X.F. Xie, S.Q. Liang, G.Z. Fang, Low-current-density stability of vanadium-based cathodes for aqueous zinc-ion batteries, Sci. Bull. 69 (2024) 833–845.

[8] Y.F. Zhang, Z.H. Zhou, X.F. Tan, Y.Y. Liu, F.F. Zhang, C.G. Meng, X.M. Zhu, Tailoring electronic structure to enhance the ammonium-ion storage properties of VO_2 by molybdenum doping toward highly efficient aqueous ammonium-ion batteries, Inorg. Chem. Front. 12 (2025) 355–368.

[9] J.N. Gong, P.F. Bai, Y.F. Zhang, Z.H. Zhou, Q.S. Wang, H.F. Lv, T. Hu, X.J. Wu, C. G. Meng, Interfacial electric field enhanced free-standing VO_2/rGO aerogel anode with ultra high mass energy density for aqueous ammonium ion battery, Small (2024) 2408467.

[10] X.F. Tan, F.F. Zhang, D.Z. Chen, J.N. Gong, J.G. Sun, C.G. Meng, Y.F. Zhang, One-step hydrothermal synthesis of vanadium dioxide/carbon core–shell composite with improved ammonium ion storage for aqueous ammonium-ion battery, J. Colloid Interface Sci. 669 (2024) 2–13.

[11] Z.H. Zhou, T.M. Lv, Z.M. Gao, D.Z. Chen, H.M. Jiang, C.G. Meng, Y.F. Zhang, Mo modulating the structure of monoclinic vanadium dioxide boosting the aqueous ammonium-ion storage for high-performance supercapacitor, J. Colloid Interface Sci. 676 (2024) 947–958.

[12] Y. Li, J. Chen, L. Su, X. Zhang, Q. Zheng, Y. Huo, D. Lin, Molybdenum-optimized electronic structure and micromorphology to boost zinc ion storage properties of vanadium dioxide nanoflowers as an advanced cathode for aqueous zinc-ion batteries, J. Colloid Interface Sci. 652 (2023) 440–448.

[13] Q. He, T. Hu, Q. Wu, C. Wang, X. Han, Z. Chen, Y. Zhu, J. Chen, J. Zhao, Tunnel-oriented VO_2 (B) cathode for high-rate aqueous zinc-ion batteries, Adv. Mater. 36 (2024) 2400888.

[14] L.L. Chen, Z.H. Yang, Y.G. Huang, Monoclinic VO_2(D) hollow nanospheres with super-long cycle life for aqueous zinc ion batteries, Nanoscale 11 (2019) 13032–13039.

[15] M.X. Bai, J.F. Gao, Z.H. He, J.F. Hou, L.B. Kong, Brookite phase vanadium dioxide (B) with nanosheet structure for superior rate capability aqueous Zn-ion batteries, J. Electroanal. 907 (2022) 116039.

[16] W.J. Li, J.R. Liang, J.F. Liu, L. Zhou, R. Yang, M. Hu, Synthesis and room temperature CH_4 gas sensing properties of vanadium dioxide nanorods, Mater. Lett. 173 (2016) 199–202.

[17] H. Liu, O. Vasquez, V.R. Santiago, L. Diaz, A.J. Rua, F.E. Fernandez, Novel pulsed-laser-deposition-VO_2 thin films for ultrafast applications, J. Electron. 34 (2005) 491–496.

[18] D.Y. Guo, Z.J. Zhao, J.B. Li, J. Zhang, R. Zhang, Z. Wang, H. Jin, Symmetric confined growth of superstructured vanadium dioxide nanonet with a regular geometrical pattern by a solution approach, Cryst. Growth Des. 17 (2017) 5838–5844.

[19] S.D. Zhang, B. Shang, J.L. Yang, W. Yan, S. Wei, Y. Xie, From VO_2 (B) to VO_2 (A) nanobelts: first hydrothermal transformation, spectroscopic study and first principles calculation, PCCP 13 (2011) 15873–15881.

[20] Y. Wang, X. Shi, J. Wang, X.Q. Liu, X.H. Lu, Nanobelt-like vanadium dioxide with three-dimensional interconnected tunnel structure enables ultrafast Al-ion storage, Mater. Today Energy 19 (2021) 100578.

[21] Y. Cai, S. Kumar, R. Chua, V. Verma, D. Yuan, Z. Kou, M. Srinivasan, Bronze-type vanadium dioxide holey nanobelts as high performing cathode material for aqueous aluminium-ion batteries, J. Mater. Chem. A 8 (2020) 12716–12722.

[22] F.Y. Kong, M. Li, X.Y. Yao, J.M. Xu, A.D. Wang, Z.P. Liu, G.H. Li, Template-free hydrothermal synthesis of VO_2 hollow microspheres, CrstEngComm 14 (2012) 3858–3861.

[23] X.C. Ren, Y.J. Zhai, L. Zhu, Y. He, A. Li, C. Guo, L. Xu, Fabrication of various V_2O_5 hollow microspheres as excellent cathode for lithium storage and the application in full cells, ACS Appl. Mater. Interfaces 8 (2016) 17205–17211.

[24] X.L. Xie, S. Wang, D.W. Gu, Z.Y. Yao, Y. Zou, X.M. Ren, Mixed-dimensional (2D/3D/3D) heterostructured vanadium oxide with rich oxygen vacancies for aqueous zinc ion batteries with high capacity and long cycling life, ACS Appl. Mater. Interfaces 16 (2024) 8679–8687.

[25] Z. Hu, L.X. Wang, K. Zhang, J. Wang, F. Cheng, Z. Tao, J. Chen, MoS_2 nanoflowers with expanded interlayers as high-performance anodes for sodium-ion batteries, Angew. Chem. Int. Ed. 53 (2014) 12794–12798.

[26] H. Hu, P.B. Zhao, X.R. Li, J. Liu, H. Liu, B. Sun, H. Cheng, Heterojunction tunnelled vanadium-based cathode materials for high-performance aqueous zinc ion batteries, J. Colloid Interface Sci. 665 (2024) 564–572.